CuCo₂S₄ Nanocrystals as A Nanoplatform for Photothermal Therapy of Arterial Inflammation

Xing Zhang [a], Junchao Liu [a], Xinrui Yang [a], Guanjie He [b], Bo Li [a,*], Jinbao Qin [a,*], Paul R. Shearing [b], Dan J. L. Brett [b], Junqing Hu [a, c, d,*], Xinwu Lu[a,*]

[a] *Department of Vascular Surgery, Shanghai Ninth People's Hospital, Shanghai Jiao Tong University School of Medicine, Shanghai 200011, China. E-mail addresses: boli@shsmu.edu.cn (B. Li); jinbaoqin@163.com (J. Qin); luxinwu@shsmu.edu.cn (X. Lu)*

[b] *Electrochemical Innovation Lab, Department of Chemical Engineering, University College London, London WC1E 7JE, UK.*

[c] *College of Materials Science and Engineering, Donghua University, Shanghai, 201620, China.*

[d] *College of Health Science and Environmental Engineering, Shenzhen Technology University, 3002 Lantian Road, Pingshan District, Shenzhen 518118, China. E-mail addresses: hu.junqing@dhu.edu.cn (J. Hu)*

Abstract：

Ultrasmall CuCo₂S₄ nanocrystals (NCs) have been demonstrated as an effective agent in the photothermal therapy (PTT) of tumors, but have not been investigated for treatment of arterial inflammation, which is critical in the initiation and development of atherosclerosis (AS), a leading cause of vascular diseases worldwide. In this study, CuCo₂S₄ NCs were synthesized and used as an efficient PTT nanoplatform for arterial inflammation. *In vitro* experiments illustrated an effective ablation of inflammatory macrophages by CuCo₂S₄ incubation combined with the irradiation of an 808 nm

near-infrared (NIR) laser. *In vivo* experiments in apolipoprotein E knockout (Apo E-/-) mice model showed the local injection with $CuCo_2S_4$ followed by irradiation with an 808 nm NIR laser notably ablated infiltrating inflammatory macrophages and effectively reduced arterial inflammation and arterial stenosis. This work provides a new strategy for treatment of AS by exploring bimetal sulfides as effective PTT agents.

Keywords: $CuCo_2S_4$ nanocrystals; Atherosclerosis; Photothermal therapy; Inflammation; Macrophages.

Introduction:

Atherosclerosis (AS) is a vascular disease affecting the most people throughout the world. As a chronic arterial disease with the severe clinical manifestations of ischemic heart disease, ischemic stroke and peripheral arterial disease, it is the major cause of global vascular death[1-4]. Recently, it has become the general consensus that arterial inflammation plays a primordial part in atherogenesis and AS development[5]. As the first clinical trial to verify this theory, the CANTOS (Canakinumab Anti-inflammatory Thrombosis Outcome Study) further confirmed a reduction of major adverse cardiac events that can be achieved by targeting the elimination of arterial inflammation[6]. While macrophages play the most critical roles in arterial inflammation, they release inflammatory factors and cytokines to accelerate atherogenesis and contribute to the thrombotic complications of AS in pivotal ways[7, 8]. Thus, it will be extremely valuable to target and eliminate the inflammatory macrophages for the prevention and treatment of AS.

In recent years, due to the rapid development of nanotechnology, photothermal therapy (PTT) using nanomaterials as photothermal reagents, especially near-infrared (NIR) laser-induced PTT, has made great progress in the treatment of various diseases with the advantage of no requirement for surgery, limited side effects, and rapid recovery[9-11]. However, most of the PTT application focused on the treatment of tumors, with only a few studies on inflammatory diseases[12-14]. Recently, Qin *et al.* and

Peng *et al.* applied PTT on inflammatory macrophages and arterial restenosis, using Au nanorods and polypyrrole nanoparticles as photothermal agents, respectively [15, 16]. Both of their studies obtained promising results, indicating PTT to be an efficacious and valid treatment option for ablation of arterial inflammation and AS.

In general, one of the prerequisites for PTT technology is the development of efficient, biocompatible, and versatile NIR light-excited photothermal conversion materials. At present, photothermal conversion materials mainly include precious metals, organic compounds, carbon materials, hybrid nanoparticles and semiconductors. Precious metal-based photothermal materials mainly include gold and palladium, but the precious metals are expensive and have unstable photothermal properties and fast degradation of performance often happens after laser irradiation [17]. Organic compound photothermal conversion materials mainly include dyes [18, 19], polyaniline[20] and polypyrrole nanoparticles[21-23]. Although such photothermal conversion materials have biodegradable properties, they are easily photodegraded or photobleached. As for carbon materials such as carbon nanotubes and graphene, despite the stable property they present, the relatively low optical absorption coefficient and complicated conditions for preparation and functionalization restricted their further development[24]. While hybrid nanoparticles such as Cu and Au hybrid nanoparticles lack reliable and reproducible synthetic procedures[25,26]. Meanwhile, semiconductor photothermal conversion materials, such as $CuCo_2S_4$ NCs, are receiving much attention due to their simple preparation, low price, stable performance and easy functionalization[27-32]. It has recently been proved that $CuCo_2S_4$ NCs are easily degraded and excreted from the body [33].

In our previous study, we synthesized ultrasmall $CuCo_2S_4$ NCs and verified their potential as a theragnostic platform for effective PTT of cancer tumors[34]. The ultrasmall $CuCo_2S_4$ NCs have the advantages of a rapid biological clearance by the renal system due to their ultrasmall size and a desirable absorbance of the NIR radiation due to an IB in their electronic band structure, which makes them a promising photothermal agent with high photothermal conversion efficiency, low cytotoxicity and low cost. While in this study, the cytotoxicity and potential utilization

of CuCo$_2$S$_4$ NCs for photothermal treatment of macrophages were investigated *in vitro*. Finally, a carotid arterial inflammation and AS model were constructed based on the ApoE−/− mice. The reduction of arterial inflammation and AS *via in vivo* treatment based on ultrasmall CuCo$_2$S$_4$ NCs was realized and the efficiency of this PTT agent were also histologically analyzed.

Experimental section

Materials

Thiourea, CuCl$_2$•2H$_2$O, CoCl$_2$•6H$_2$O and poly(vinyl pyrrolidone) (PVP, K30) were purchased from Sinopharm Chemical Reagent Co., Ltd. (Shanghai, China) and used without further purification. Methoxypoly(ethylene glycol) amine (PEG-NH$_2$) was purchased from Sigma-Aldrich. The mouse macrophage cell line, Raw264.7, was purchased from the ScienCell Research Laboratories (Carlsbad, CA, USA). High glucose (4500 mg L^{-1}) Dulbecco's modified eagle medium (DMEM), fetal bovine serum, penicillin and streptomycin were purchased from Gibco Company. The other chemical reagents were purchased from Shanghai Chemical Reagent Research Institute Co. Ltd (Shanghai, China). The deionized (DI) water was acquired from a Milli-Q Direct Water Purification System (Merck KGaA, Darmstadt, Germany) with the resistivity at 25 °C of 18.2 MΩ cm.

Synthesis and characterization of ultrasmall CuCo$_2$S$_4$ NCs

CuCl$_2$•2H$_2$O (0.25 mmol), CoCl$_2$•6H$_2$O (0.5 mmol), thiourea (1.5 mmol) and poly (vinyl pyrrolidone) (PVP, K30) were mixed and dissolved in 30 mL deionized (DI) water under magnetic stirring. Then, 100 μL ethylenediamine was slowly added to the above solution. Finally, the resulting solution was transferred to a stainless steel autoclave, sealed, and heated at 160 °C for 20 h. A black precipitate was collected by centrifugation and washed with ethanol and deionized water several times. To improve the biocompatibility of the CuCo$_2$S$_4$ NCs, the NCs were further modified by coating a layer of PEG-NH$_2$, and purified by centrifugation.

The morphology, size and microstructure of $CuCo_2S_4$ NCs were determined by a transmission electron microscope (JEM-2010F; Japan). XRD measurements were performed on a D/max-2550 PC X-ray diffractometer (XRD; Rigaku, Japan). UV-vis absorbance spectra and diffuse reflectance spectra were measured at room temperature using a UV-visible-NIR spectrophotometer operating from 200 to 1000 nm (Shimadzu UV-3600; Japan). Contents of ions released from as-synthesized $CuCo_2S_4$ NCs were determined by an inductively coupled plasma atomic emission spectroscopy (ICP-AES; Prodigy; USA). Fourier transform infrared (FTIR) spectra were measured using an infrared spectrometer (Nicolet 6700; USA). The 808 nm semiconductor lasers were purchased from Shanghai Xilong Optoelectronics Technology Co. Ltd., China, whose power could be adjusted externally (0-2 W). The output power of lasers was independently calibrated using a hand-held optical power meter (Newport model 1918-C, CA, USA).

To measure the photothermal performance, 100 μL of $CuCo_2S_4$ NCs with various concentrations were irradiated by an 808 nm semiconductor laser device at a power density of 0.5 W cm^{-2} for 5 min. To evaluate the photostability of the NCs, the samples were irradiated with 808 nm laser for 5 min (LASER ON), followed by naturally cooling without irradiation for 5 min (LASER OFF). This cycle repeated for five times. The temperature was monitored and imaged simultaneously by a thermal imaging camera (FLIR A300, USA).

Cell culture, TEM detection and cell viability assay

High glucose DMEM supplemented with 10 % fetal bovine serum was used to culture the mouse macrophage cell line Raw264.7 according to the instructions. Then, Raw264.7 macrophages were identified using the macrophage-specific antibody

CD68 (Abcam, UK) both by immunofluorescence and flow cytometry. Next, TEM assay was performed by first coculturing Raw264.7 macrophages with 80 μg mL^{-1} CuCo$_2$S$_4$ NCs for 12 h, followed by irradiating half of them with 808 nm NIR laser. After which, irradiated and unirradiated macrophages were collected for TEM detection, as previously described[35]. Thus, the phagocytosis of CuCo$_2$S$_4$ NCs by macrophages and the ablation of macrophages by 808 nm NIR laser was observed. Then *in vitro* cell viability assays of Raw264.7 macrophages was performed. First, the CCK8 cell proliferation assay (Dojindo Laboratories, Kumamoto, Japan) was used to evaluate the cytotoxicity of CuCo$_2$S$_4$ NCs against Raw264.7 macrophages. Macrophages were co-cultured using different concentrations of CuCo$_2$S$_4$ NCs (0, 10, 20, 40, 80, 120, 200, 400 and 800 μg mL^{-1}) for 12 h, and then CCK8 cell proliferation assay was used to detect macrophage survival rate, shown in previous work[36]. Then the safe concentration on macrophages was chosen for the following experiments. Next, Raw264.7 macrophages were incubated using different concentrations of CuCo$_2$S$_4$ NCs (0, 40, 80 and 120 μg mL^{-1}) for 12 h, then half of them were irradiated for 5 min using an 808 nm NIR laser at a power density of 0.56 W cm^{-2}. In another comparison experiments, Raw264.7 macrophages were incubated with CuCo$_2$S$_4$ NCs (80 μg mL^{-1}) for 12 h and then irradiated with the 808 nm NIR laser at different power densities (0, 0.28, 0.56 and 1.12 W cm^{-2}) for 5 min. The cell viability was determined using the CCK-8 cell proliferation assay. At the same time, the cells treated as above were stained with calcein AM / PI (Dojindo Laboratories, Shanghai, China) and a Zeiss LSM 510 META immunofluorescence microscope (Carl-Zeiss-Strasse, Oberkochen. Germany) was used to observe and take photos. In all of the above experiments, macrophages were washed with PBS after co-culturing with CuCo$_2$S$_4$ NCs.

Animal model and *in vivo* thermal therapy

All animal experiments were approved by the Animal Ethics Committee of the Shanghai Jiaotong University, School of Medicine. 16 eight-week-old apolipoprotein E knockout (Apo E - / -) mice (C57 BL6 background) fed with a high-fat diet (21%

fat, 0.15% cholesterol) were purchased from Shanghai Southern Model Biotechnology Co., Ltd. (Shanghai, China) for subsequent experiments. First, after using sodium pentobarbital (40 mg kg^{-1}) to anaesthetize the mice, the tissue was incised to expose both sides of the carotid artery and placed a constrictive polyethylene collar (Milaty, Zhangjiagang, China) surrounding the right carotid artery, as reported previously[37]. Isolation from the tissue was also done to the contralateral left carotid artery, but no collar was placed around as a self-control (sham operation group). 14 days after the surgery, the PBS solution with CuCo$_2$S$_4$ NCs (80 μg mL^{-1}, 100 μL) was locally injected into 8 mice with carotid stenosis (the CuCo$_2$S$_4$ group), and injected an equal volume of PBS into the other 8 control mice (the PBS group). 12 hours after the injection, an 808 nm NIR laser with a power density of 0.56 W cm^{-2} was used for vertical irradiation of the two groups. Finally, an infrared (IR) imager (GX-300; Shanghai Infratest Electronics Co., Shanghai, China) was applied to monitor the body temperature and record the real-time infrared thermal images.

Histological analysis and blood analysis

14 days after PTT, the mice were sacrificed. First, the bilateral carotid arteries of all mice were extracted, frozen sections were prepared and immunofluorescence staining was performed. Macrophages were stained with CD68 (Abeam, UK), smooth muscle cells (SMC) were stained with SMA (Abeam, UK), and nuclei with 6-dimercapto-2-phenylindole (DAPI) (DAKO, USA). At the same time, a paraffin-embedded section of the carotid artery was prepared and hematoxylin/eosin (HE) staining was performed to observe and record images of the carotid intima and media, then ImageJ Pro Plus software (NIH, Bethesda, MD, http://www.imagej.nih.gov) was used to analyze the thickness of the carotid intima and media. Moreover, HE staining on the heart, liver, spleen, lung, kidney and small intestine was also performed to analyze the biotoxicity of CuCo$_2$S$_4$ NCs on the major organs. Finally, the blood from both 8 treated mice and 8 age-matched healthy mice was collected to evaluate the biocompatibility of CuCo$_2$S$_4$ NCs. Thereby, the biocompatibility of CuCo$_2$S$_4$ NCs in the blood circulation system was evaluated.

Statistics

All quantitative data from the experiments were reported in the form of mean ± standard deviation (SD). Student's t-test or one-way analysis of variance (ANOVA) was applied to determine the statistical significance ($P<0.05$) of the data. All experiments were repeated at least three times in every group.

Results and discussion

A facile hydrothermal method was used to prepare $CuCo_2S_4$ NCs using polyvinylpyrrolidone (PVP) as a surfactant and surface ligand to make the NCs hydrophilic. To improve the biocompatibility of $CuCo_2S_4$ NCs upon macrophages, the NCs were further modified by coating a layer of PEG-NH$_2$, evidenced by Fourier transform infrared spectrum (Fig. S1). The end NCs could remain stable when dispersed in water, PBS, and RPMI-1640 culture medium for a week (Fig. S2A). The nanosheets retained their strong NIR absorption at room temperature for a week, indicating good dispersion in water/PBS/RPMI-1640 culture medium (Fig. S2B-D). The morphology and size of the end $CuCo_2S_4$ NCs were measured by transmission electron microscopy (TEM). As shown in Figures 1A, $CuCo_2S_4$ NCs are spherical particles with a size of about 14 nm. To confirm the crystallographic structure, the NCs were then measured by powder X-ray diffraction (XRD). As shown in Figure 1B, the pattern could be well indexed to the cubic spinel $CuCo_2S_4$ phase (JCPDS no. 42-1450). Light absorption in the NIR region is a prerequisite for NIR-induced PTT agents. Materials with strong NIR absorption are considered to be good photothermal agents for PTT. Fig. 1C displays the UV-vis-NIR absorbance spectrum of the aqueous dispersion. They exhibited a strong NIR absorption from 700 nm to 1000 nm. By determining the $CuCo_2S_4$ NC concentration using ICP-AES, the extinction coefficient of the $CuCo_2S_4$ NCs at 808 nm was measured to be 16.2 L g^{-1}cm^{-1}. Under continuous laser irradiation of 808 nm wavelength, the aqueous dispersion of NCs at different concentration shows a dramatic and smooth elevation of temperature with an increase of the solution concentration (Fig. 1D). The photothermal conversion efficiency can

be calculated to be 68.8% (Fig. S3). Also, the as-prepared NCs showed great NIR photostability upon a long time irradiation by an 808 nm laser (Fig. S4). These indicated that $CuCo_2S_4$ NCs are excellent PTT agents and have potential application in *in vivo* cell ablation.

As recorded, macrophages are the most important effector cells in chronic arterial inflammation, which leads to AS[38-40]. The prerequisite of ablating macrophages is whether they can uptake the ultrasmall $CuCo_2S_4$ NCs. Hence, the macrophage-specific marker CD68 was first used to identify Raw264.7 mouse macrophages (Fig. S5, see ESI†). Then, TEM results demonstrated that macrophages co-incubated with $CuCo_2S_4$ NCs demonstrated significant phagocytosis compared to normal macrophages (Fig. 2A and 2D), and no significant organelle injuries were observed (Fig. 2B and 2E). Nevertheless, after 12 h of coculturing with 80 μg mL^{-1} $CuCo_2S_4$ NCs and 5 min exposure to an 808 nm NIR laser at a power density of 0.56 W cm^{-2}, Raw264.7 macrophages demonstrated obvious nuclear lysis and cytolysis. The specific manifestations were dissolution and fragmentation of the nucleus, the disappearance of nucleoli and endoplasmic reticulum (Fig. 2C and F). The results of the TEM assay indicated that PTT could effectively ablate and eliminate macrophage to death. Therefore, $CuCo_2S_4$ NCs could act as a PTT agent that kill macrophages and reduce arterial inflammation infiltration.

A cytotoxicity test was then performed to determine that $CuCo_2S_4$ NCs could be safely used in biomedical and clinical research. First, $CuCo_2S_4$ NCs was incubated with Raw264.7 macrophages for 12 hours. It was found that there was no significant difference in cell viability between $CuCo_2S_4$ NCs group and control group (Fig. 3A) under the concentration of 200 μg mL^{-1}. Therefore, $CuCo_2S_4$ NCs below a concentration of 120 μg mL^{-1} were selected for co-incubation with macrophages in subsequent experiments to ensure its biosafety.

Next, the effects of concentration and NIR laser power density on cell viability was analyzed to explore the optimal $CuCo_2S_4$ NCs concentration and the power density of the 808 nm NIR laser. Cell viability was determined using the CCK-8 cell proliferation assay, and live/dead cells were stained with calcein AM/PI and examined

under a fluorescence microscope. The results showed that the viability of Raw264.7 cells progressively decreased with the increase of laser power density, but the power density of 0.56 W cm^{-2} was similar to the maximum value of 1.12 W cm^{-2}, which was safer and could ablate the macrophages by over 90% (Fig. 3B). With the increase of CuCo$_2$S$_4$ NCs concentration, the cell viability also decreased progressively. The cell viability was the highest at 0 μg mL^{-1}, and the lowest at 120 μg mL^{-1}, but the ablation effect that a safer concentration of 80 μg mL^{-1} was similar to that achieved by 120 μg mL^{-1} (Fig. 3C). The calcein AM/PI staining results of live/dead cells were consistent with the results of the CCK8 assay (Fig. 3D). These results imply that CuCo$_2$S$_4$ NCs are a safe, low toxic photothermal material that could be combined with 808 nm NIR laser irradiation to effectively ablate Raw264.7 macrophages *in vitro*. The results of *in vitro* PTT suggests the need for further exploration of *in vivo* models of arterial inflammation and atherosclerosis.

The atherogenesis and atherosclerotic plaque progression begin from the interaction between the blood vessel endothelium and cardiovascular risk factors, hemodynamic forces, toxins, and pathogens, which leads to the decrease of nitric oxide (NO) production and the increase of endothelial monolayer permeability. The subsequent endothelial cell injury causes the up-regulation of leukocyte adhesion molecules, thereby macrophages and leukocytes increasingly adhere to the endothelial cells and enter the subendothelial layer through the endothelium gaps along with lipoproteins due to the increased endothelial monolayer permeability. Chemokines and cytokines like interleukin-8 (IL-8) further promote leukocytes and smooth muscle cells (SMCs) recruitment to enter the subendothelial layer. Subendothelial macrophages and SMCs then start taking in surrounding lipoproteins which have been oxidized and become foam cells. Necrotic foam cells in the center of the progressive atheromatous plaque become a central lipid core with SMCs, macrophages and other leukocytes in the periphery. Furthermore, other cytokines like transforming growth factor-β (TGF-β) promote subendothelial SMCs migration, collagen formation, and fibrotherus cap formation. The fact that atherosclerosis is an inflammatory disease is now widely accepted and the immune system takes part all along atherogenesis and

atherosclerosis progression[41,42]. Therefore, reducing macrophage infiltration may inhibit the development of arterial inflammation and atherosclerosis.

ApoE(-/-) mice fed with a high-fat diet was applied, and placed a tightened polyethylene collar around the right common carotid artery, which induced local chronic arterial inflammation, stenosis and atherosclerosis through a 2-week compression of the collar. Then, a solution of $CuCo_2S_4$ NCs (80 μg mL^{-1}, 100 μL) was percutaneously injected into the tissues surrounding the carotid artery of the experimental group (the $CuCo_2S_4$ group), and an equal volume of PBS was injected into the same position of the control group (the PBS group). After 12 h, local irradiation (0.56 W cm^{-2}) was performed on the neck using an 808 nm NIR laser. At the same time, temperature changes in the whole body was recorded using an infrared camera (Fig. 4A). Within 5 minutes, the local surface temperature of the $CuCo_2S_4$ group progressively increased from ~ 25 ° C to ~ 57 ° C, while that of the PBS control group increased slightly (Fig. 4B). The above results confirmed the excellent photothermal effect of $CuCo_2S_4$ NCs.

Next, 14 days after PTT, the carotid arteries of the sacrificed mice were prepared into frozen sections and paraffin sections, which were subjected to immunofluorescence staining and HE staining, respectively, and observed under a microscope. The macrophage-specific antibody CD68 was used to label infiltrating macrophages in carotid arteries, and used vascular smooth muscle cell-specific antibody α-SMA to label the carotid SMCs to observe the co-localization of macrophages and SMCs. The PBS control group demonstrated a significant infiltration of macrophages (Fig. 5A i and ii), while the $CuCo_2S_4$ + NIR group (Fig. 5A iii and iv) and the sham operation group (Fig. 5A v and vi) showed significantly less macrophage infiltration (Fig. 5A v and vi). Moreover, there was no significant difference in the relative quantity of macrophages between the $CuCo_2S_4$ + NIR group and the sham operation group (Figure 5B). The above results confirmed that $CuCo_2S_4$ NCs as a photothermal agent could effectively ablate macrophages and reduce chronic inflammation of the carotid artery.

HE staining and ImageJ Pro Plus software analysis of the intima and media

thickness of the carotid arteries showed a significant reduction in intima and media thickness of the $CuCo_2S_4$ + NIR group (Fig. 6A iii and iv) compared to the PBS control group (Fig. 6A i and ii). There was no significant difference in intima and media thickness comparing the $CuCo_2S_4$ + NIR group and the sham operation group (Fig. 6A v and vi), the above experimental results showed that PTT could be significantly improved by eliminating arterial inflammation of $CuCo_2S_4$ NCs as a photothermal agent (Fig. 6B). The intrinsic reason may be that the SMCs co-existing in the intimal layer with macrophages were in the proliferative phase, and the higher temperature inhibited the proliferation, thereby inducing SMCs death, thus preventing arterial intimal hyperplasia and stenosis, and preventing and treating atherosclerosis. Moreover, in the entire *in vivo* experiment, complications such as thrombosis or bleeding were not observed. Therefore, local injection of $CuCo_2S_4$ NCs followed by irradiation of 808 nm NIR laser is safe and effective for the prevention and treatment of arterial inflammation and stenosis of atherosclerosis.

As a safe and qualified PTT agent, good biocompatibility is an important prerequisite. 14 days after PTT, mice in both groups were sacrificed. HE staining was subsequently performed on major organs. There were no significant differences in heart, liver, spleen, lung, kidney and intestine between $CuCo_2S_4$ + NIR group and PBS control group, and no obvious lesions, such as injury or inflammation, were observed (Fig. 7). It was proved that $CuCo_2S_4$ NCs have no obvious toxicity to major organs. The chemical components of the blood samples of the two groups was analyzed, and it is found that the alanine aminotransferase (ALT) (Fig. S6A, see ESI†), aspartate aminotransferase (AST) (Fig. S6B), total bilirubin (T-Bil) (Fig. S6C), and blood urea nitrogen (BUN) (Fig. S6D) levels in the blood of both groups were not significantly different. It was proved that $CuCo_2S_4$ NCs had no significant side effect on liver and kidney function. In summary, $CuCo_2S_4$ NCs had no obvious side effects on mice and was a safe and qualified PTT agent for the living body.

Conclusions

This study has successfully synthesized and characterized the ultrasmall

CuCo$_2$S$_4$ NCs with the advantage of high photothermal efficiency, nontoxic and good biocompatibility. *In vitro* experiments demonstrated an effective ablation of inflammatory macrophages by CuCo$_2$S$_4$ incubation combined with irradiation of 808 nm near-infrared (NIR) laser light. *In vivo* experiments in apolipoprotein E knockout (Apo E-/-) mice model showed that local injection with CuCo$_2$S$_4$ followed by irradiation with 808 nm NIR laser notably ablated infiltrating inflammatory macrophages and effectively reduced arterial inflammation and arterial stenosis. Although the exploration of the optimal CuCo$_2$S$_4$ NCs concentration, the optimal power density and the long-term incidence of complications are still needed, our study has proved that ultrasmall CuCo$_2$S$_4$ NCs is a promising nanoplatform for PTT of arterial inflammation and stenosis under 808 nm NIR laser irradiation, which is potentially a new approach for the prevention and treatment of AS.

Acknowledgments

References

1.   W. Herrington, B. Lacey, P. Sherliker, J. Armitage and S. Lewington, *Circ. Res.*, 2016, **118**, 535-546.
2.   A. E. Moran, M. H. Forouzanfar, G. A. Roth, G. A. Mensah, M. Ezzati, C. J. Murray and M. Naghavi, *Circulation*, 2014, **129**, 1483-1492.
3.   I. Abubakar, T. Tillmann and A. Banerjee, *Lancet*, 2015, **385**, 117-171.
4.   S. J. Curry, A. H. Krist, D. K. Owens, M. J. Barry, A. B. Caughey, K. W. Davidson, C. A. Doubeni, J. W. Epling, A. R. Kemper and M. Kubik, *JAMA*, 2018, **320**, 177-183.
5.   P. Libby, *Arterioscl. Throm. Vas.*, 2012, **32**, 2045-2051.
6.   P. M. Ridker, B. M. Everett, T. Thuren, J. G. MacFadyen, W. H. Chang, C. Ballantyne, F. Fonseca, J. Nicolau, W. Koenig and S. D. Anker, *New Engl. J. Med.*, 2017, **377**, 1119-1131.
7.   J. W. Williams, C. Giannarelli, A. Rahman, G. J. Randolph and J. C. Kovacic, *J. Am. Coll. Cardiol.*, 2018, **72**, 2166-2180.
8.   K. J. Moore, S. Koplev, E. A. Fisher, I. Tabas, J. L. Björkegren, A. C. Doran and J. C. Kovacic, *J. Am. Coll. Cardiol.*, 2018, **72**, 2181-2197.

9. J. C. Li, C. Xie, J. G. Huang, Y. Y. Jiang, Q. Q. Miao and K. Y. Pu, *Angew. Chem. Int. Edit.*, 2018, **57**, 3995-3998.

10. J. C. Li, X. Zhen, Y. Lyu, Y. Y. Jiang, J. G. Huang and K. Y. Pu, *ACS Nano*, 2018, **12**, 8520-8530.

11. Y. J. Liu, Z. Yang, X. L. Huang, G. C. Yu, S. Wang, Z. J. Zhou, Z. Y. Shen, W. P. Fan, Y. Liu, M. Davisson, H. Kalish, G. Niu, Z. H. Nie and X. Y. Chen, *Acs Nano*, 2018, **12**, 8129-8137.

12. H. Kosuge, S. P. Sherlock, T. Kitagawa, R. Dash, J. T. Robinson, H. Dai and M. V. McConnell, *J. Am. Heart Assoc.*, 2012, **1**, e002568.

13. H. Lee, M.-Y. Lee, S. H. Bhang, B.-S. Kim, Y. S. Kim, J. H. Ju, K. S. Kim and S. K. Hahn, *ACS nano*, 2014, **8**, 4790-4798.

14. H. Pan, R. U. Palekar, K. K. Hou, J. Bacon, H. Yan, L. E. Springer, A. Akk, L. Yang, M. J. Miller and C. T. Pham, *Int. J. Nanomedicine*, 2018, **13**, 5187.

15. J. Qin, Z. Peng, B. Li, K. Ye, Y. Zhang, F. Yuan, X. Yang, L. Huang, J. Hu and X. Lu, *Nanoscale*, 2015, **7**, 13991-14001.

16. Z. Peng, J. Qin, B. Li, K. Ye, Y. Zhang, X. Yang, F. Yuan, L. Huang, J. Hu and X. Lu, *Nanoscale*, 2015, **7**, 7682-7691.

17. Z. Zhang, J. Wang and C. Chen, *Adv. Mater.*, 2013, **25**, 3869-3880.

18. Q. Chen, C. Wang, Z. Zhan, W. He, Z. Cheng, Y. Li and Z. Liu, *Biomaterials*, 2014, **35**, 8206-8214.

19. W. R. Chen, R. L. Adams, S. Heaton, D. T. Dickey, K. E. Bartels and R. E. Nordquist, *Cancer Lett.*, 1995, **88**, 15-19.

20. J. Zhou, Z. Lu, X. Zhu, X. Wang, Y. Liao, Z. Ma and F. Li, *Biomaterials*, 2013, **34**, 9584-9592.

21. Z. Zha, X. Yue, Q. Ren and Z. Dai, *Adv. Mater.*, 2013, **25**, 777-782.

22. M. Chen, X. Fang, S. Tang and N. Zheng, *Chem. Commun.*, 2012, **48**, 8934-8936.

23. K. Yang, H. Xu, L. Cheng, C. Sun, J. Wang and Z. Liu, *Adv. Mater.*, 2012, **24**, 5586-5592.

24. M. H. Lan, S. J. Zhao, Z. Y. Zhang, L. Yan, L. Guo, G. L. Niu, J. F. Zhang, J. F. Zhao, H. Y. Zhang, P. F. Wang, G. Y. Zhu, C. S. Lee and W. J. Zhang, *Nano Res*, 2017, **10**, 3113-3123.

25. D. Zhu, M. Liu, X. Liu, Y. Liu, P. N. Prasad and M. T. Swihart, *J Mater Chem B*, 2017, **5**, 4934-4942.

26. M. J. Sailor and J. H. Park, *Adv Mater*, 2012, **24**, 3779-3802.

27. Z. Chen, Q. Wang, H. Wang, L. Zhang, G. Song, L. Song, J. Hu, H. Wang, J. Liu and M. Zhu, *Adv. Mater.*, 2013, **25**, 2095-2100.

28. S. Goel, F. Chen and W. Cai, *Small*, 2014, **10**, 631-645.

29. W. Li, R. Zamani, P. Rivera Gil, B. Pelaz, M. Ibáñez, D. Cadavid, A. Shavel, R. A. Alvarez-Puebla, W. J. Parak and J. Arbiol, *J. Ame. Chem. Soc.*, 2013, **135**, 7098-7101.

30. J. M. Luther, P. K. Jain, T. Ewers and A. P. Alivisatos, *Nat. Mater.*, 2011, **10**, 361.

31. L. Cheng, J. Liu, X. Gu, H. Gong, X. Shi, T. Liu, C. Wang, X. Wang, G. Liu

and H. Xing, *Adv. Mater.*, 2014, **26**, 1886-1893.

32. D. L. Ni, J. W. Zhang, J. Wang, P. Hu, Y. Y. Jin, Z. M. Tang, Z. W. Yao, W. B. Bu and J. L. Shi, *ACS Nano*, 2017, **11**, 4256-4264.

33. J. Liu, P. Wang, X. Zhang, L. Wang, D. Wang, Z. Gu, J. Tang, M. Guo, M. Cao and H. Zhou, *ACS nano*, 2016, **10**, 4587-4598.

34. B. Li, F. Yuan, G. He, X. Han, X. Wang, J. Qin, Z. X. Guo, X. Lu, Q. Wang, I. P. Parkin and C. Wu, *Adv. Funct. Mater.*, 2017, **27**, 1606218.

35. J. Qin, K. Li, C. Peng, X. Li, J. Lin, K. Ye, X. Yang, Q. Xie, Z. Shen and Y. Jin, *Biomaterials*, 2013, **34**, 4914-4925.

36. X. Liu, B. Li, F. Fu, K. Xu, R. Zou, Q. Wang, B. Zhang, Z. Chen and J. Hu, *Dalton Trans.*, 2014, **43**, 11709-11715.

37. R. Puranik, S. Bao, E. Nobecourt, S. J. Nicholls, G. J. Dusting, P. J. Barter, D. S. Celermajer and K.-A. Rye, *Atherosclerosis*, 2008, **196**, 240-247.

38. G. Fredman and I. Tabas, *Am. J. Pathol.*, 2017, **187**, 1211-1221.

39. Z. A. Fayad, F. K. Swirski, C. Calcagno, C. S. Robbins, W. Mulder and J. C. Kovacic, *J. Am. Coll. Cardiol.*, 2018, **72**, 2198-2212.

40. K. J. Lavine, A. R. Pinto, S. Epelman, B. J. Kopecky, X. Clemente-Casares, J. Godwin, N. Rosenthal and J. C. Kovacic, *J. Am. Coll. Cardiol.*, 2018, **72**, 2213-2230.

41. A. N. Sidawy and B. A. Perler, *Rutherford's Vascular Surgery and Endovascular Therapy, 2-Volume Set*, *Elsevier Health Sciences*, 2018.

42. K. J. Moore and I. Tabas, *Cell*, 2011, **145**, 341-355.

Figure legends:
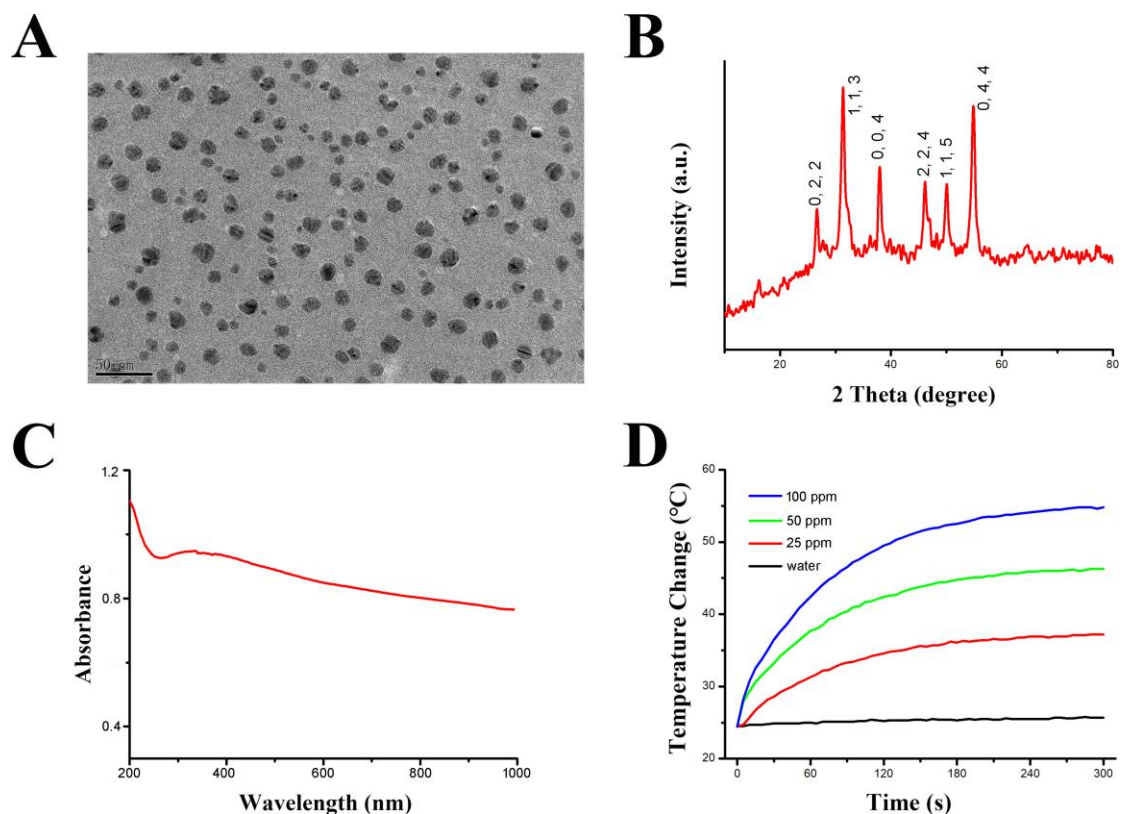
Figure 1. (A) Typical low-magnification TEM image of as-synthesized $CuCo_2S_4$ NCs. (B) Powder XRD patterns of the as-prepared $CuCo_2S_4$ NCs. (C) UV-vis-NIR absorption spectrum of the $CuCo_2S_4$ NC solution at room temperature. (D) Photothermal effect of $CuCo_2S_4$ NCs in aqueous solution at different concentrations.
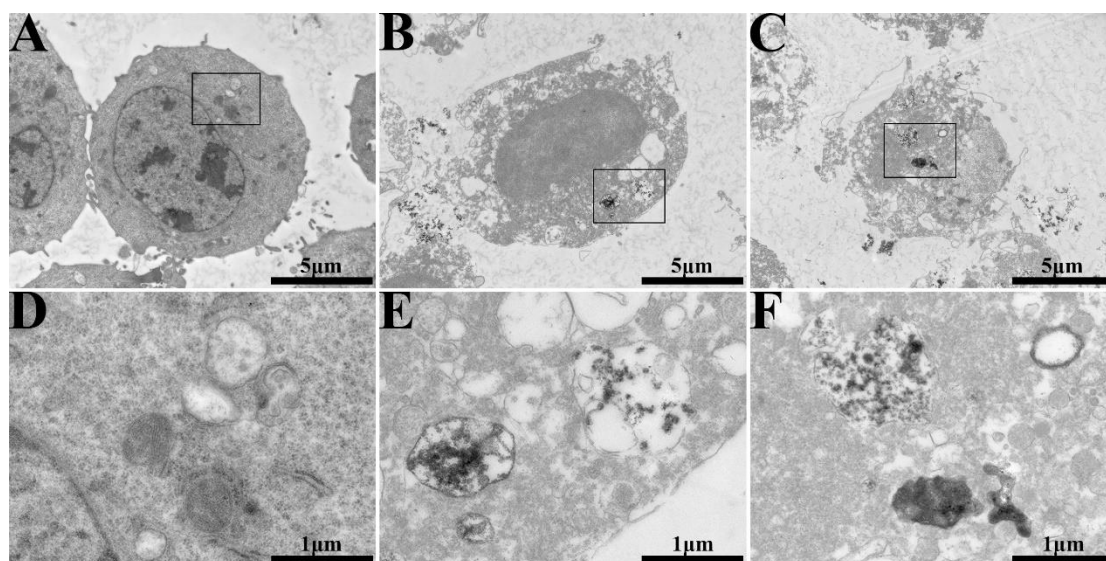
Figure 2. TEM images of Raw264.7 macrophages with or without CuCo$_2$S$_4$ NCs and laser irradiation. (A) Normal macrophages without CuCo$_2$S$_4$ NCs. (B) Macrophages co-incubated with 80 μg mL^{-1} CuCo$_2$S$_4$ NCs demonstrated significant phagocytosis of CuCo$_2$S$_4$ NCs and no significant organelle injuries was observed. (C) After 12 h of coculturing with 80 μg mL^{-1} CuCo$_2$S$_4$ NCs for and 5 min exposure to an 808 nm NIR laser at a power density of 0.56 W cm^{-2}, Raw264.7 macrophages demonstrated obvious nuclear lysis and cytolysis, namely dissolution and fragmentation of the nucleus, disappearance of nucleoli and endoplasmic reticulum. (D) High magnification of image (A). (E) High magnification of image (B). (F) High magnification of image (C).
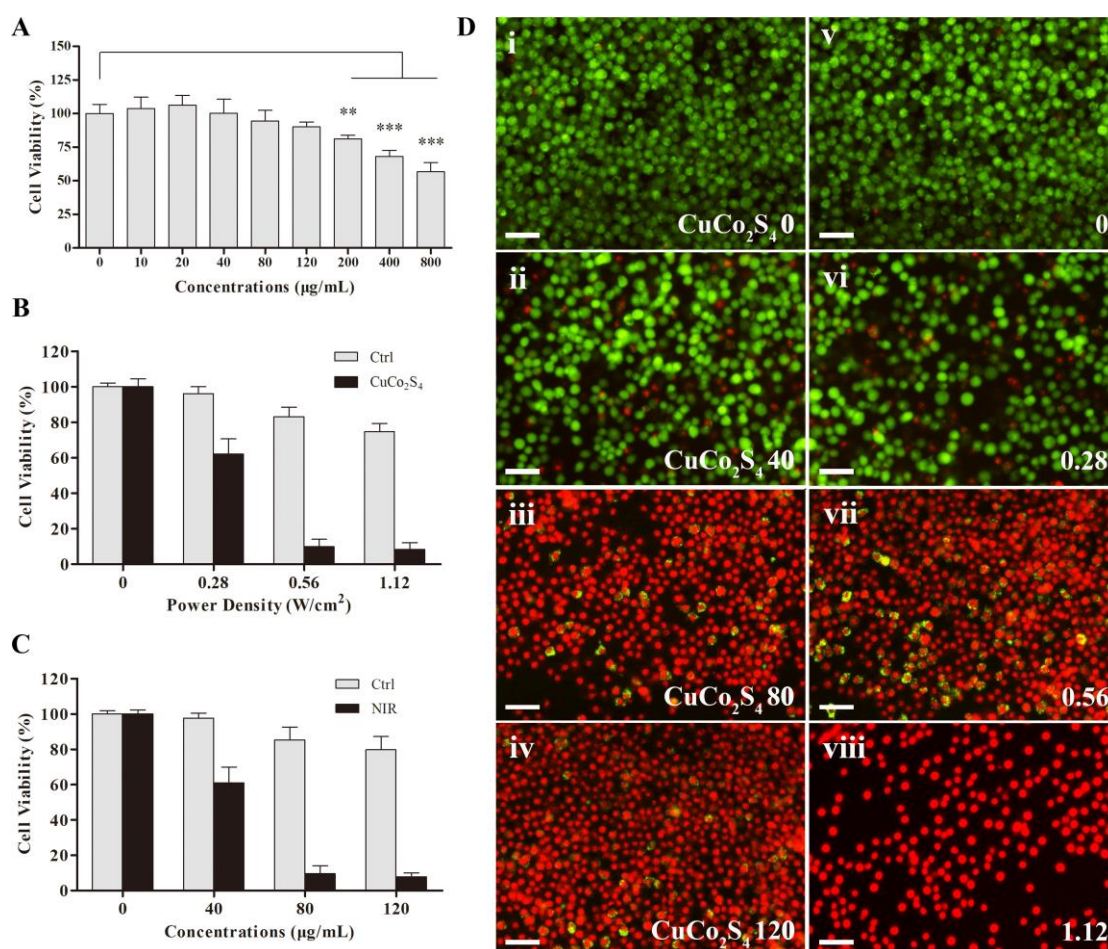
Figure 3. Cytotoxicity of CuCo$_2$S$_4$ NCs and PTT, and in vitro PTT effect of CuCo$_2$S$_4$

NCs in combination with 808 nm NIR laser irradiation on Raw264.7 macrophages. (A)

In vitro relative cell viability of Raw264.7 macrophages cocultured with or without

various concentrations of CuCo$_2$S$_4$ NCs for 12 h. (B) Relative viabilities of Raw264.7

macrophages under NIR laser irradiation at different power densities (0, 0.28, 0.56,

and 1.12 W cm^{-2}) alone (grey) or after incubation with the CuCo$_2$S$_4$ NCs (80 μg mL^{-1})

(black). (C) Relative viabilities of Raw264.7 macrophages after incubation with the

CuCo$_2$S$_4$ NCs at different concentrations (0, 40, 80, and 120 μg mL^{-1}) alone (grey) or

followed by the NIR laser irradiation (0.56 W cm^{-2}) after incubation (black). (D)

Representative images of Calcein AM (green)/PI (red) staining for living (green)/dead (red) cells after incubation with the $CuCo_2S_4$ NCs at different concentrations followed by NIR laser irradiation (0.56 W cm^{-2}) or under different power densities after incubation with the $CuCo_2S_4$ NCs (80 μg mL^{-1}). All scale bars are 50 μm.
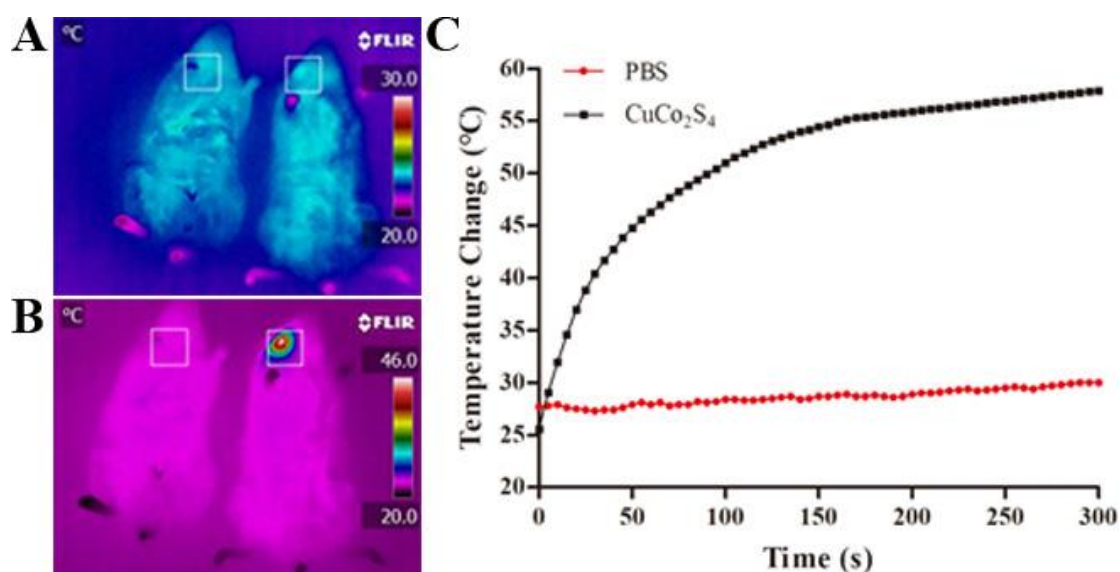
Figure 4. Photothermal therapy on a mouse model using $CuCo_2S_4$ NCs in combination with 808 nm NIR laser irradiation. (A) Infrared thermal images of two mice injected with either the $CuCo_2S_4$ NCs (the right one, indicated region 12) or PBS (the left one, indicated region 11), respectively, irradiated with the 808 nm laser (0.56 W cm^{-2}) for 60 s. (B) Temperature changes in regions 11 and 12 as a function of the irradiation time.
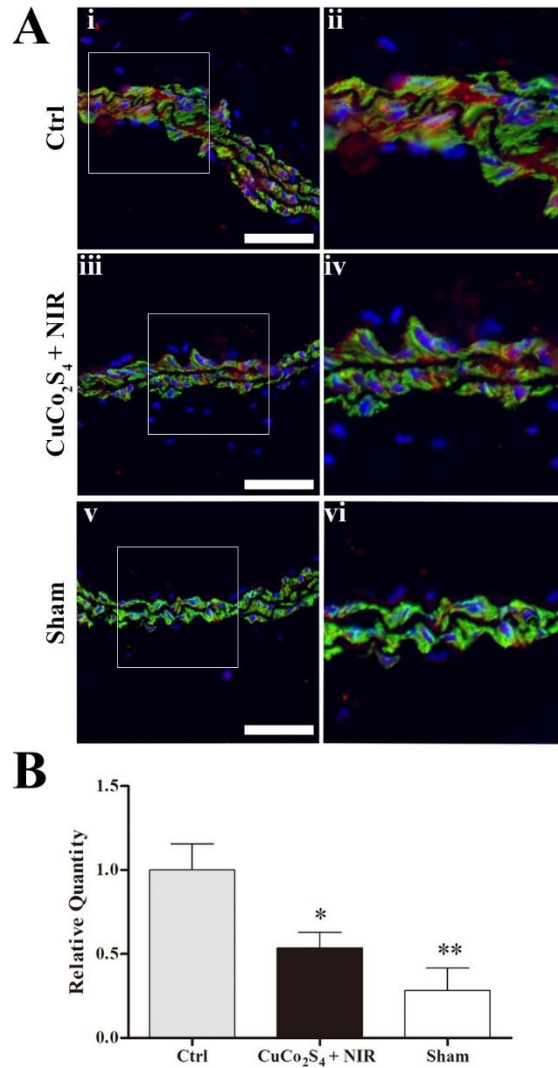
Fig 5. Histological analysis of carotid artery inflammation in a mouse model. (A) i, iii, and v are representative images of SMA (green) and CD68 (red) co-staining in collar-implanted group mice with injection of PBS and NIR laser irradiation (control), collar-implanted group mice with the $CuCo_2S_4$ NCs injection and NIR laser irradiation ($CuCo_2S_4$ NCs + NIR), and sham-operated mice (Sham), respectively. ii, iv, and vi are high magnification images of i, iii, and v, respectively. (B) Statistics. All scale bars = 50 μm. *: $P < 0.05$, **: $P < 0.01$.
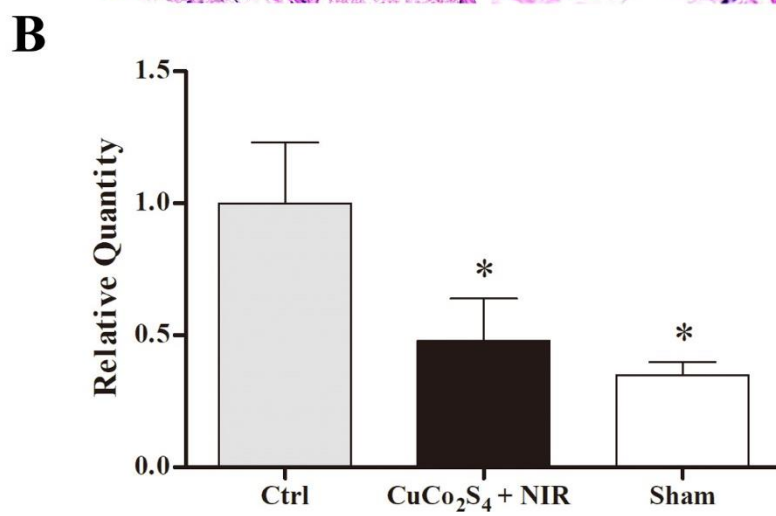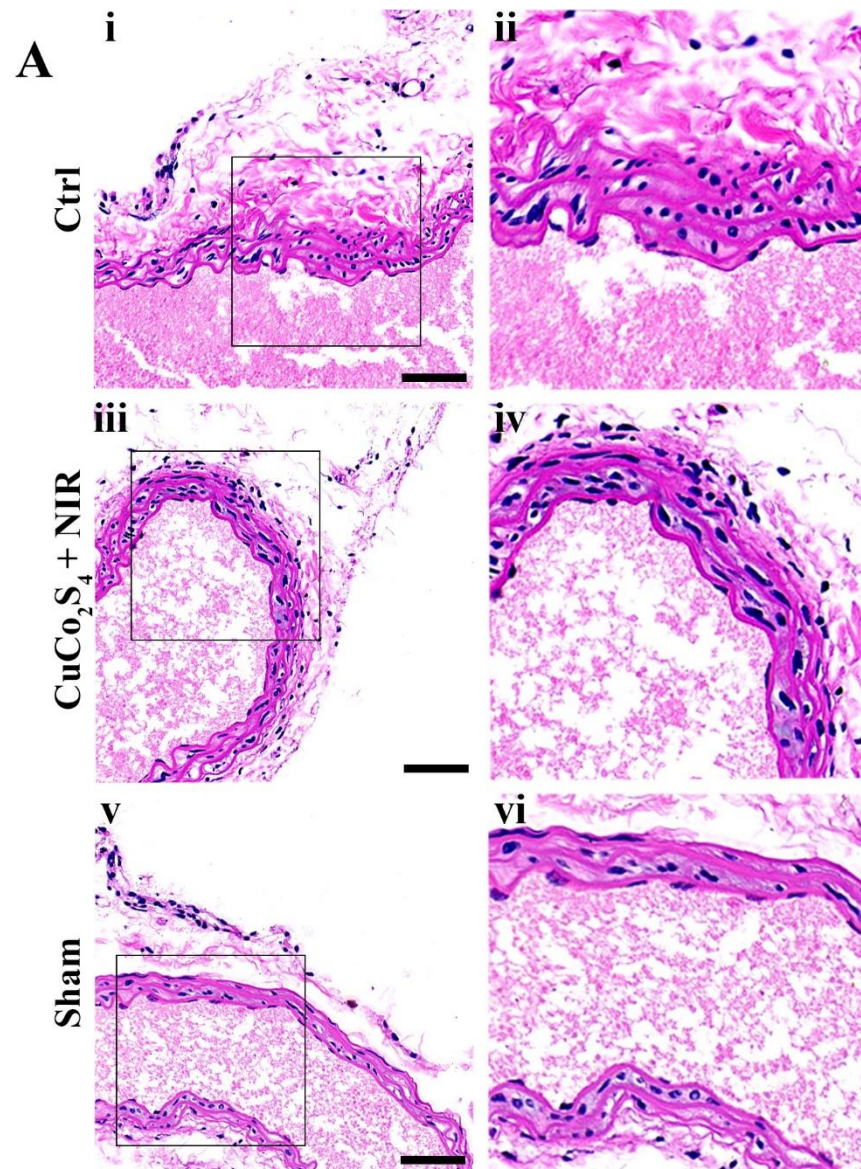
Fig 6. Histological analysis of carotid artery stenosis in a mouse model. (A) i, iii, and

v are representative images of HE images of carotid artery thickness in collar-implanted group mice with PBS injection and NIR laser irradiation(control), collar-implanted group mice with the $CuCo_2S_4$ NCs injection and NIR laser irradiation ($CuCo_2S_4$ NCs + NIR), and sham-operated mice (Sham), respectively. ii, iv, and vi are high magnification images of i, iii, and v, respectively. (B) Statistics. All scale bars = 100 μm. *: $P < 0.05$.
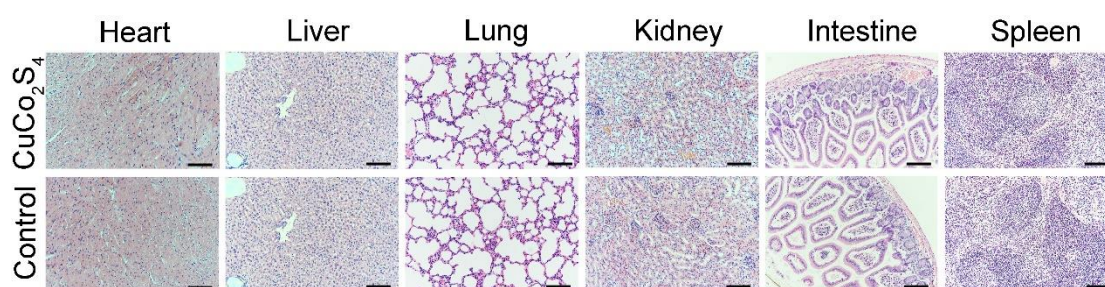
Fig 7. Representative images of HE staining of the main visceral organs in the Apo E - / - mice treated with the $CuCo_2S_4$ NCs after the PTT. There were no significant differences in heart, liver, spleen, lung, kidney and intestine between $CuCo_2S_4$ + NIR group and PBS control group, and no obvious lesions such as injury or inflammation were observed. All scale bars = 100 μm.

The table of contents entry

Our study proved ultrasmall $CuCo_2S_4$ nanocrystals is a promising nanoplatform for photothermal therapy of arterial inflammation.